Australian Meteorological and Oceanographic Journal 61 (2011) 253–267

The Antarctic ozone hole during 2010

A.R. Klekociuk[1], M.B. Tully[2], S.P. Alexander[1], R.J. Dargaville[3], L.L. Deschamps[4], P.J. Fraser[4], H.P. Gies[5], S.I. Henderson[5], J. Javorniczky[5], P.B. Krummel[4], S.V. Petelina[6], J.D. Shanklin[7], J.M. Siddaway[6] and K.A. Stone[6]

[1]Climate Processes and Change, Australian Antarctic Division, Australia
[2]Bureau of Meteorology, Australia
[3]School of Earth Sciences, Melbourne University, Australia
[4]Centre for Australian Weather and Climate Research—A partnership between the Australian Bureau of Meteorology and CSIRO, Australia
[5]Australian Radiation Protection and Nuclear Safety Agency, Australia
[6]Department of Physics, La Trobe University, Australia
[7]British Antarctic Survey, United Kingdom

(Manuscript received August 2011)

The Antarctic ozone hole of 2010 is reviewed from a variety of perspectives, making use of various data and analyses. Based on total column ozone metrics, the 2010 ozone hole was one of the smallest in the past fifteen–twenty years. The main influence on the size of the ozone hole was relatively warm temperatures in the Antarctic lower stratosphere which impeded ozone depletion in the austral spring. The warm winter temperatures were associated with a significant dynamical disturbance in the mid- and high latitude upper stratosphere during July which included a substantial warming of the mid- and upper extratropical stratosphere, a deceleration of zonal winds and a cooling in the polar mesosphere. The disturbance was likely influenced by the phase of the Quasi-Biennial Oscillation (QBO) which favoured a weak and disturbed polar vortex in the winter months. The winter warming also resulted in significant off-pole displacement and weakening of the polar vortex in the mid- to upper stratosphere, producing a long-lasting increase in the overburden of ozone and weakening ozone hole metrics based on total column ozone measurements. Ozone loss in the lower stratosphere was less markedly affected by this dynamical activity, and was similar to other recent years. A notable feature was the reduction in dynamical disturbances of the polar vortex after September, when the QBO moved into a strongly eastward phase. During the late spring and early summer, stratospheric temperatures warmed more slowly than in recent years, and this produced one of the longest-lasting ozone holes yet observed which eventually disappeared in the last week of December. The relatively low ozone levels in December resulted in unusually high surface ultraviolet fluxes as measured on the coast of East Antarctica.

Introduction

The amount of ozone in the stratosphere has been significantly influenced over the past five decades by the atmospheric abundance of man-made ozone depleting substances (WMO 2011a). Severe loss of stratospheric ozone associated with the so-called ozone hole continues to occur each spring over Antarctica as it has done annually since around 1980 (Farman et al. 1985; Stolarski et al. 1986; Hassler et al. 2011). Meteorological factors continue to play a significant role in the interannual variability of the size and severity of the Antarctic ozone hole (WMO 2011a). However as shown by Salby et al. (2011), when account is made for variability driven by the propagation of planetary waves into the polar stratosphere, indications of ozone recovery are emerging. In the Arctic, less severe but overall significant ozone loss has been observed in boreal spring since the

Corresponding author address: A.R. Klekociuk, Climate Processes and Change, Australian Antarctic Division, 203 Channel Highway, Kingston Tas. 7050, Australia
email: andrew.klekociuk@aad.gov.au

early 1990s (WMO 2011a; Sonkaew et al. 2011), with losses during early 2011 being the largest yet observed (Manney et al. 2011) due to unusually cold atmospheric conditions.

Understanding of the causes and influences of stratospheric ozone depletion continues to be advanced through observational studies, laboratory measurements and modelling (WMO 2011a). Characterisation of the formation conditions for Polar Stratospheric Clouds (PSC) have been significantly advanced in the past few years by space-borne remote sensing measurements, particularly by the Cloud-Aerosol Lidar and Infrared Pathfinder Satellite Observations (CALIPSO) satellite mission (e.g. Alexander et al. 2011; Khosrawi et al. 2011; Pitts et al. 2011), and associated chemistry measurements by satellite-borne remote-sensing missions, such as Aura, ODIN and ENVISAT, and in-situ sampling. Knowledge of stratospheric chemical processes continues to be improved, particularly through the testing of uncertainties in chemical reaction kinetics by combining various observational data sets with laboratory measurements (e.g. Kawa et al. 2009; Sumińska-Ebersoldt et al. 2011). Simulation of PSC aerosols and stratospheric chemical reactions in stratosphere resolving chemistry-climate models are now relatively mature (e.g. SPARC CCMval 2010; Kirner et al. 2011). In the climate modelling arena, recent studies have continued to demonstrate the important role that stratospheric ozone depletion has played in influencing the climate of the southern hemisphere and the Antarctic region, particularly in the austral summer (e.g. Perlwitz et al. 2008; Gillett et al. 2009; Waugh et al. 2009a,b; Karpechko et al. 2010; McLandress et al. 2010; Son et al. 2010; SPARC CCMVal 2010; Arblaster et al. 2011; Deushi and Shibata 2011; Hu et al. 2011; Forster et al 2011; Kang et al. 2011; McLandress et al. 2011; Ndarana et al. 2011; Polvani et al. 2011a,b; Sigmond et al. 2011). A particular emphasis of work in the modelling community continues to be the accurate simulation of stratospheric thermodynamics, particularly in relation to minimising biases in Antarctic winter temperatures, and adequately treating feedbacks from dynamical processes associated with wave-induced momentum transfer and mixing (SPARC CCMVal 2010; WMO 2011a).

In this paper we provide an overview of the Antarctic ozone hole and southern hemisphere stratospheric conditions in 2010 from various perspectives and present a range of Australian data and analyses including Bureau of Meteorology (BoM) meteorological analyses, ozone data from satellites analysed by the Commonwealth Scientific and Industrial Research Organisation (CSIRO) Marine and Atmospheric Research division, ozone profiles from Antarctica obtained from the Australian Antarctic Division (AAD) and BoM ozonesonde program, and Antarctic ultraviolet measurements from the Australian Radiation Protection and Nuclear Safety Agency (ARPANSA) biometer network. A variety of data from satellite missions and ground-based instruments are also presented. We focus on a description of meteorological conditions and their relation to the overall level of Antarctic ozone depletion in 2010. This work complements analyses of previous Antarctic ozone holes reported by Tully et al. (2008, 2011).

Meteorological conditions

Polar temperatures and atmospheric indices

From January to June of 2010, monthly mean temperatures in the lower stratosphere above Antarctica were generally below normal. The left panels of Fig. 1 show monthly temperature anomalies for the latitude range 90°S to 65°S from the National Centers for Environmental Prediction (NCEP) Reanalysis-2 data (Kanamitsu et al. 2002) with respect to the base period 1979–1999 for three pressure levels. At 100 hPa, mean temperatures for May and June were the lowest observed for all corresponding months since 1979, and the anomalies for these months for 50 hPa were at or near the lowest corresponding monthly values since 2001. In contrast, a warming began in June that became strongest in the upper levels (Fig. 1) during July. At 10 hPa, the July anomaly was the warmest of that month for the decade since 2001. The warm (positive) anomaly persisted into August at this level, and was also observed at 50 hPa from July to September. As discussed below, this disturbance was related to the development of strong planetary wave activity. The warming during the austral winter subsided during the early spring, with a return to relatively cold temperatures from October. December was notable in having the coldest 50 hPa and 100 hPa anomalies for this month since 1979.

During 2010, the NCEP standardised 30 hPa Quasi-Biennial Oscillation (QBO) index (http://www.cpc.ncep.noaa.gov/data/indices/qbo.u30.index) shifted from a strongly negative (westward) anomaly in the months up to June (with values for February to June being at the lowest corresponding monthly extremes since 1979) to a strongly positive (eastward) anomaly by the end of the year (Fig. 1, top right panel). The QBO modulates the ability of upward propagating planetary waves to influence extratropical latitudes. A weaker and more disturbed polar vortex is preferentially observed during the negative (westward) QBO phase (Baldwin and Dunkerton 1998). The QBO values suggest that dynamical disturbance of the high-latitude stratosphere was more likely during the early winter, during which the QBO was in the negative phase

The surface standardised Southern Annular Mode index (Marshall 2003 and http://www.antarctica.ac.uk/met/gjma/sam.html) vacillated during the year (Fig. 1, bottom right panel), but was strongly positive in June, July, October and November, being at or near the corresponding monthly extremes observed since 1979. The surface SAM expresses the sense of meridional pressure gradient anomalies, with positive (negative) values indicating anomalous positive (negative) pressure gradients between mid- and high latitudes. As discussed in Baldwin and Dunkerton (2001), positive

Fig. 1 Left: Monthly temperature anomalies (K) from zonal means for the latitude range 90°S to 65°S from NCEP Reanalysis-2 data relative to the monthly climatology for 1979–1999 at pressure levels of 10 hPa (top), 50 hPa (middle) and 100 hPa (bottom). Coloured bars show monthly anomalies for 2010, and diamonds connected by solid lines show maximum and minimum anomalies for 1979–2010. Numbers at the top of each panel are the rank of 2010 relative to years 2001–2010 (1 [10] = most positive [most negative] anomaly), and numbers at the bottom of each panel are values (K) of the monthly anomalies for 2010. Right: (top) NCEP standardised 30 hPa Quasi-Biennial Oscillation (QBO) index and (bottom) standardised surface Southern Annular Mode (SAM) index (Marshall 2003). Both indices are expressed in standard deviations relative to base period of 1981–2010 (for QBO) and 1971–2000 (for SAM). Diamonds connected by solid lines show maximum and minimum anomalies for each index over the period 1979–2010.

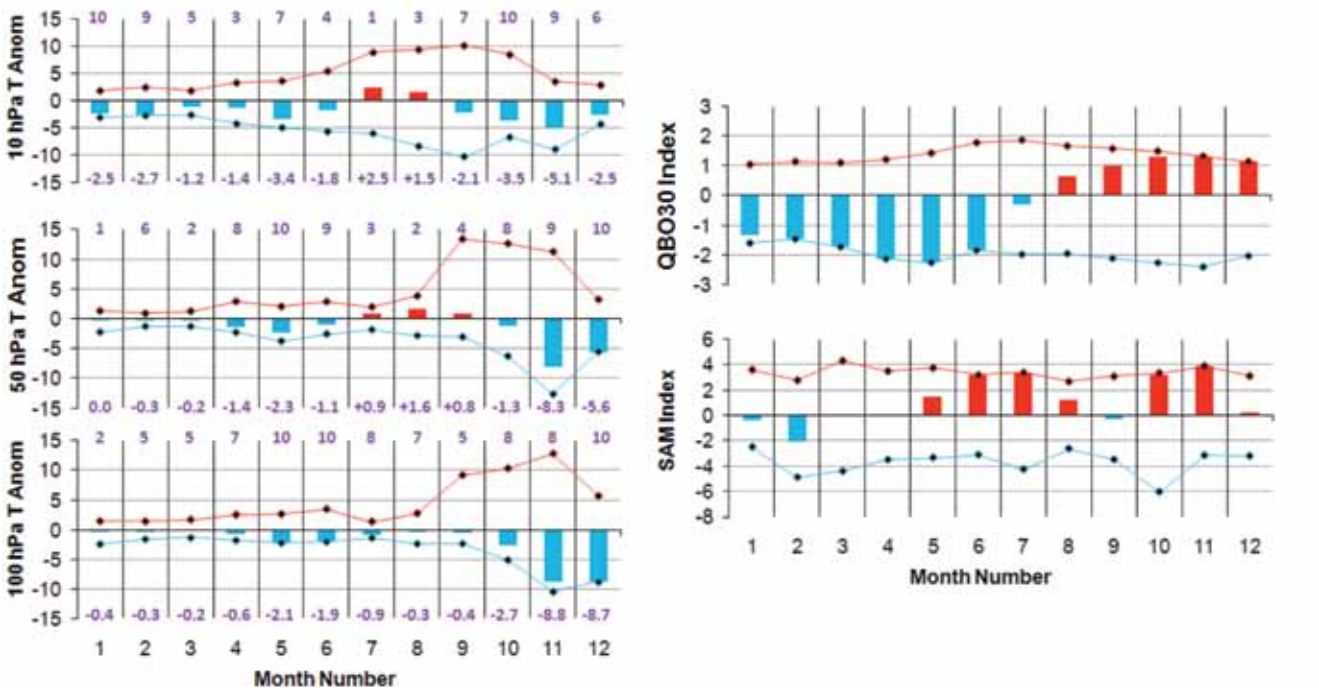

(negative) anomalies in the stratospheric SAM tend to occur preferentially under conditions of a strong (weak) polar vortex (corresponding to positive (negative) QBO phase). Stratospheric and tropospheric SAM variations are sometimes independent, but as noted in Baldwin and Dunkerton (2001), SAM anomalies just above the tropopause tend to favour tropospheric SAM anomalies of the same sign. As shown in the right panels of Fig. 1, SAM and QBO were of opposite sign in winter but both strongly positive in October and November.

Dynamical activity in July

Figure 2 shows the time-height temperature cross section above the South Pole during 2010 from the Australian Community Climate and Earth System Simulator (ACCESS) numerical weather prediction (NWP) analysis on the global domain (ACCESS-G). The warming during the austral winter months noted above can be identified in Fig. 2 during mid-June and from mid-July through to early August in the cold core of the stratospheric polar vortex at pressures less than 200 hPa.

Further information on the vertical structure of the winter warming can be gleaned from Fig. 3 which shows mean daily zonal mean temperatures for the latitude range 85°S to 65°S from measurements by the Microwave Limb Sounder (MLS) onboard the Aura spacecraft. A general warming is apparent between heights of approximately 20 km to 60 km from late June, with the largest temperature change at the stratopause (~55 km height) in late July and early August. Associated with the warming episode was a pronounced cooling between heights of approximately 65 km and 85 km. Subsequent smaller episodes of stratospheric warming and mesospheric cooling can be seen from mid-September to late November. In the Modern Era Retrospective-reanalysis for Research and Applications (MERRA) (Reinecker et al. 2011) native resolution product, the zonal average zonal balanced winds above 65 km at 69°S showed a pronounced reduction coincident with the July–August stratospheric warming (not shown). Siskind et al. (2010), has shown in a model study that mesospheric cooling and zonal wind reduction accompanying stratospheric warmings are potentially produced by a reduction of the residual downward circulation in the mesosphere due to stratospheric critical level filtering of orographic gravity waves.

The general warming of the Antarctic stratosphere during July occurred during the development of strong zonal asymmetries in temperature and wind velocity above 35 km height which reached from southern mid-latitudes to the pole. A quasi-stationary wavenumber 1 planetary wave pattern in zonal temperature appeared around 17 July and intensified over the following two weeks. As shown in Figure 4(a) for the 2.2 hPa pressure level in the United

Fig. 2 Daily time-pressure section of air temperature at 90°S from the global domain of the Australian Community Climate and Earth System Simulator (ACCESS) numerical weather prediction model. The black contour delineates the 195 K contour, which is the approximate warmest formation threshold for Polar Stratospheric Clouds.

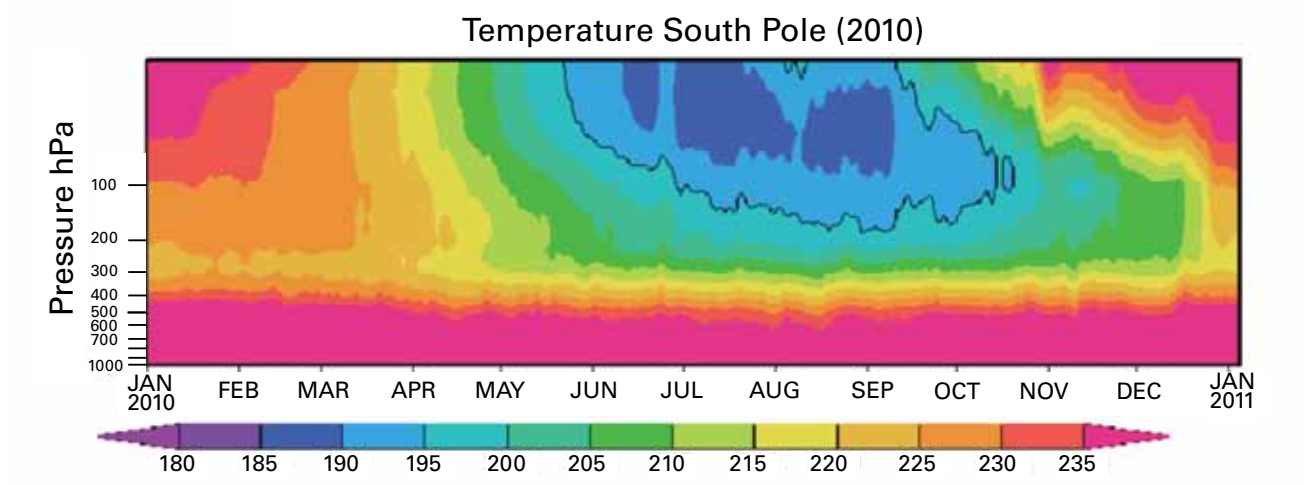

Fig. 3 Daily time-height section of zonal average air temperature for latitudes 85°S to 65°S from Aura Microwave Limb Sounder (MLS) version 3.3 data for 2010. The black and white contours delineate the formation threshold of Nitric Acid Trihydrate (NAT) and water-ice aerosols, respectively, calculated using MLS chemistry data. The NAT threshold contour in the winter stratosphere indicates the potential seasonal and vertical extent of type I Polar Stratospheric Clouds. The region enclosed by the water-ice cloud threshold (above 80 km height in December) is associated with the cold summer mesopause region.

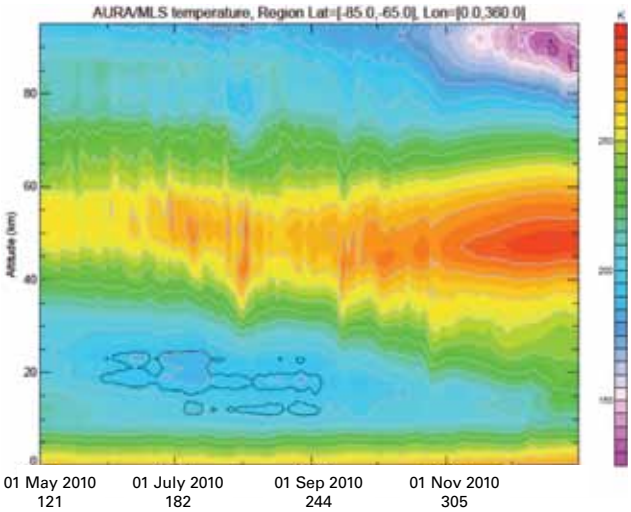

Kingdom Meteorological Office (UKMO) stratospheric assimilation (Swinbank and O'Neill 1994), the cold pool that normally resides over the pole was displaced towards South America. In the lower stratosphere, the corresponding UKMO temperature field was more zonally symmetric (Fig. 4(b)), although showing a persistent warm ridge near 45°S that stretched eastwards from near 90°E to east of South America. This ridge showed both quasi-stationary wave-1 behaviour in the Australian sector, and eastward drifting wave-2 features.

Fig. 4 Analyses of gridded data from Stratospheric Assimilated Data of the United Kingdom Meteorological Office (UKMO). Shown by coloured contours is temperature at (a) 2.2 hPa and (b) 50 hPa. Lines with arrowheads show wind direction; from tip to head is the approximate distance covered in two hours of time.

(a)

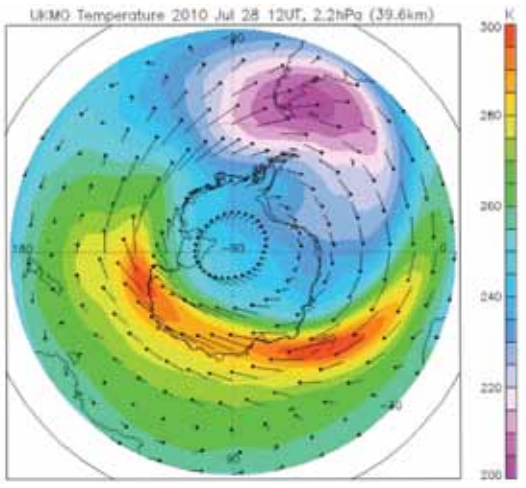

(b)

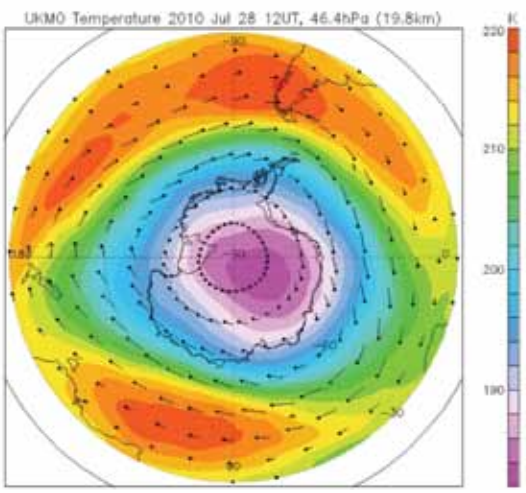

The July disturbance resulted in strongly asymmetric meridional heat transport in the southern hemisphere. In Fig. 5, a jet of warm air in the mid-stratosphere (labelled 'A') connecting mid-latitudes to Antarctica can be seen moving progressively eastward and poleward in late July and early August. Zonally averaged, poleward heat transport at this time was strongest in the upper stratosphere and lower mesosphere, and particularly at mid-latitudes, as shown in Fig. 6. A further significant heat flux episode occurred in September.

At Davis station in Antarctica (68.6°S, 78.0°E), Rayleigh lidar measurements provided high vertical and temporal resolution information on the vertical structure of the disturbance. As shown in Fig. 7(a), the stratopause was relatively warm and low (at 45 km height) in late July, with relatively cool conditions in the lower mesosphere at the same time (similar to the situation in the polar cap average shown in Fig. 3). In the mid-stratosphere (near 30–40 km height), the temperature anomaly with respect to the climatological mean for 1979–2009 exceeded 30 K (Fig. 7(b)), and the warm anomaly near this height was significant at the 5th percentile with respect to the climatology during late June and all of July. An additional warming in the lower stratosphere (near 20 km) and stratopause (near 60 km) can be seen in September, corresponding to the timing of features noted in Figs 3 and 6. An accompanying cold anomaly near 35 km and in the mesosphere suggests that at Davis this disturbance had a vertical wavelength on the order of 40 km.

The polar vortex

The structure of the polar vortex on the 500 K isentropic surface is shown in Fig. 8. The vortex edge was at –70 to –72 degrees equivalent latitude during June 2010, which was 5 to 8 degrees further toward the pole than during June 2008 or June 2009 (Tully et al., 2011). The vortex centre shifted equatorward by around 10 degrees in equivalent latitude in

Fig. 5 Eddy heat flux (the product of the zonal anomalies of meridional wind and temperature) on the 2.2 hPa pressure surface at two-day intervals evaluated from UKMO Stratospheric Assimilated Data. Top: (left) 26 July, (right) 28 July. Bottom: (left) 30 July, (right) 1 August. Label 'A' identifies the region where the warm zonal temperature anomaly is moving southward (negative values). Label 'B' relates to regions where cold anomalies are either moving northward (negative values) or southward (positive values), or warm anomalies are moving northward (positive values). Note that Fig. 4(a) shows the corresponding temperature map for the top right panel.

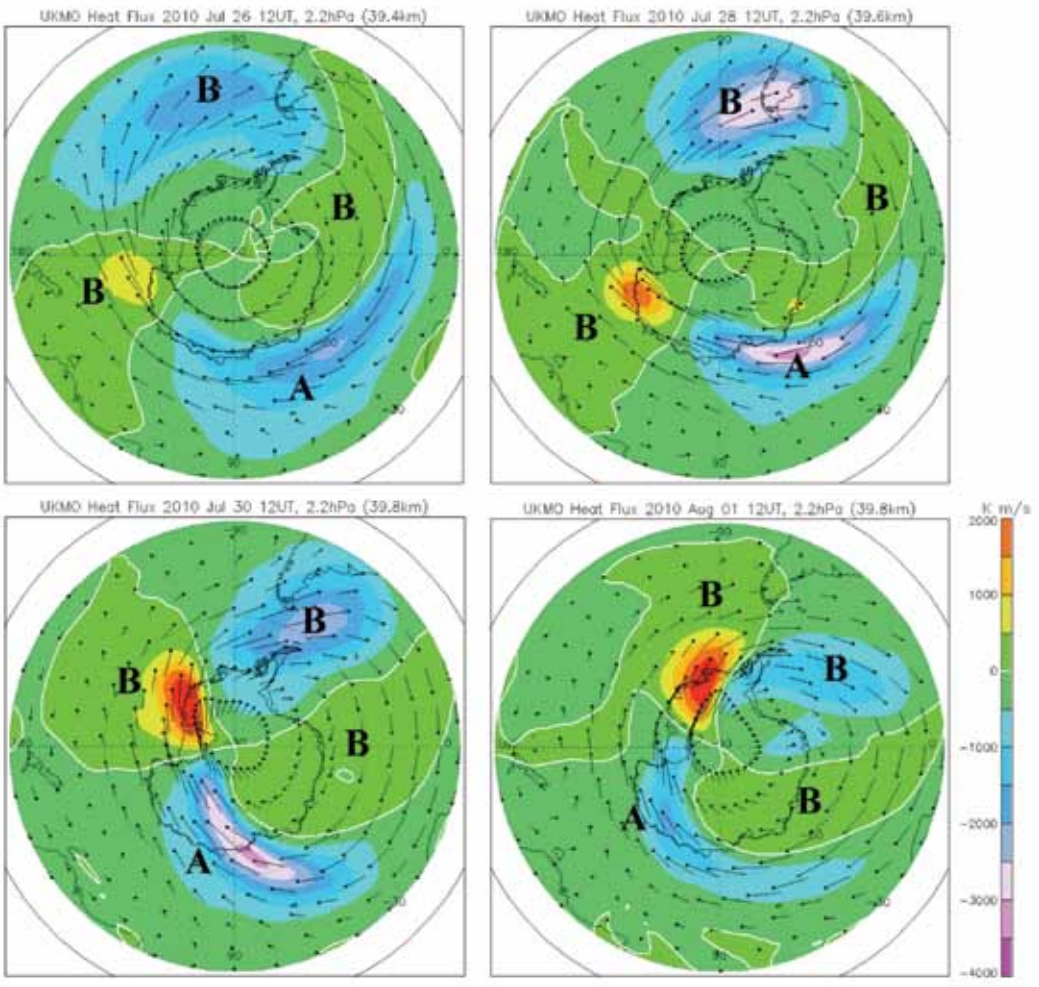

Fig. 6 Daily eddy heat flux averaged between latitudes of (top) 55°S to 35°S and (bottom) 85°S and 65°S as a function of pressure evaluated from UKMO Stratospheric Assimilated Data. Negative values indicate poleward transport of heat. The zero contour is outlined in white. In the top panel, values less than –600 K m s^{-1} have been set to the lowest contour level; the minimum value during the strong negative event in late July was –701 K m s^{-1}.

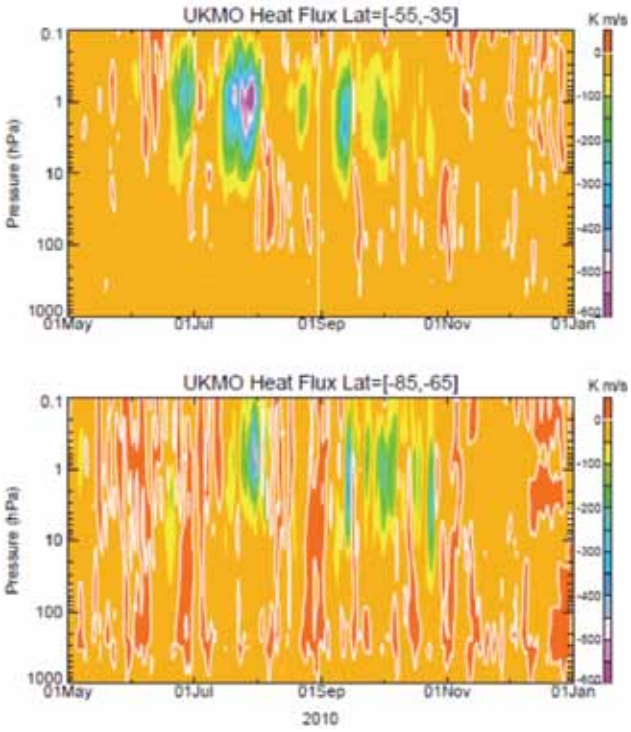

mid-July. Figure 8 also shows the location of Davis station with respect to the vortex edge; Davis was close to the vortex edge until mid-July, then subsequently approximately 15 degrees inside the edge for most of the remainder of the year. The equivalent latitudinal gradient in potential vorticity and the position of the vortex edge during spring 2010 was similar to the structure of the two previous Antarctic vortices (Tully et al. 2011).

Figures 9(a) and 9(b) show the area of the vortex during 2010 on the 450 K and 850 K potential temperature isentropic surfaces, respectively, in comparison with climatological data for 1992–2009. At 450 K (near 18 km height, and near the region of maximum springtime ozone loss), the vortex area was consistently greater than the climatological mean throughout the year, and particularly so during November and December when new extreme maximum climatological values were set. The unusually large vortex area values occurred during the time the 30 hPa QBO index was in an extreme positive phase (Fig. 1) and conducive to reduced dynamical disturbance of the polar stratosphere. Anomalously low polar cap temperatures in the lower stratosphere also occurred at this time (left panels of Fig. 1). The persistence of the vortex may also have influenced the timing of the transition from winter to summer conditions

Fig. 7 (a)Time-height section of daily average air temperature above Davis station, Antarctica (69.6°S, 78.0°E) from May to November 2010, obtained from Rayleigh lidar measurements (above 27 km height) augmented with radiosonde measurements. The original measurements have been interpolated to a uniform grid with resolution 1 km in height and five days in time; vertical lines near the top of the graph show the times of the original measurements. The top 5 km of each lidar profile has been removed to allow for convergence of the lidar retrieval. The graph at right shows the mean standard error of the original measurements as a function of height. (b) Time-height temperature difference graph obtained by subtracting a climatological mean from the original measurements in (a) and gridding as for (a). The climatology (covering heights to 80 km) was interpolated from Modern Era Retrospective-reanalysis for Research and Applications (MERRA) native resolution air temperature data for the period 1979–2009. Diagonal hatching covers regions having temperatures less than the 5th percentile or greater than the 95th percentile with respect to the climatology. The white contour is at 0 K. The graph at right shows the mean difference as a function of height, with vertical dashed lines at 10 K intervals. Above approximately 60 km height, MERRA (which uses GEOS5 atmospheric model) tends to be biased cold by approximately 10 K or more (see Fig. 26 of Schwartz et al. 2008) and this accounts for most of the difference in the upper heights.

(a)

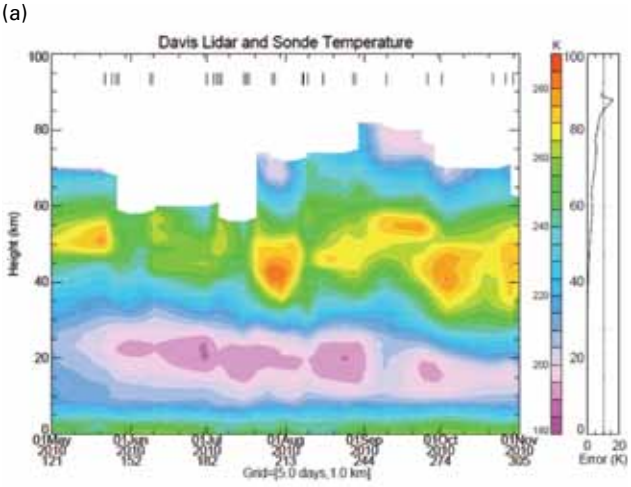

(b)

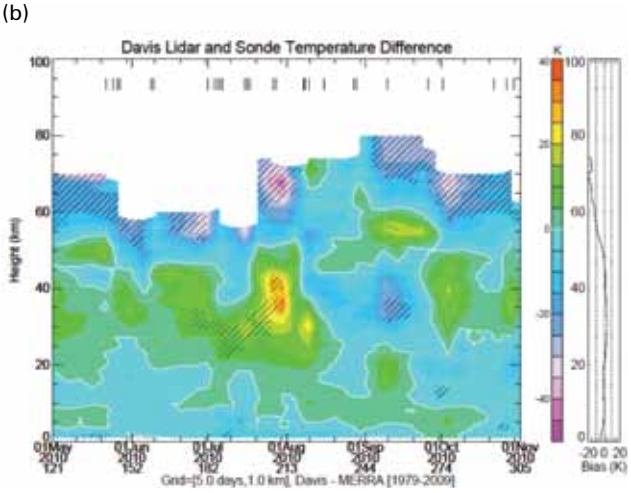

Fig. 8 Potential vorticity gradient (expressed in PVU per degree of equivalent latitude) as a function of time and equivalent latitude for the 500 K potential temperature isentrope (~20 km height), derived from the UKMO stratospheric assimilation. Equivalent latitude is derived using the method of Nash et al. (1996). The white contour denotes the equivalent latitude of Davis station (68.6°S, 78.0°E). Additional red contours show the location of the 'inner', 'central', and 'outer' limits of the vortex edge as defined by Nash et al. (1996).

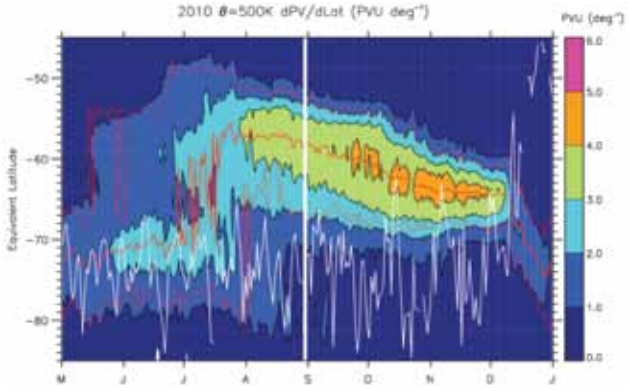

in the Antarctic mesosphere (Kirkwood et al. 2008): the date at which the water-ice threshold was reached in the mesosphere shown in Fig. 3 (3 December) was approximately two weeks later than in 2009, and the mesospheric cold point in early December was generally 3–5 km higher than in 2009 (not shown).

A hiatus in the growth rate of the vortex occurred during July during the time of the enhanced planetary wave activity and warming of the upper stratosphere discussed above. At 850 K (near 31 km height), the vortex area was less than the climatological mean up to mid-May, and exceeded the climatological mean in June and to a lesser extent in July. At the end of July the vortex area anomalously declined and remained near the climatological 5th percentile until September, after which it followed the climatological mean.

Figure 10 shows the long-term behaviour of the mean vortex area for a selected month on each of the levels of Fig. 9. In Fig. 10(a), it can be seen that the 450 K vortex area in December 2010 was similar to that in 2001 and 2006, which were years of strong and stable vortices. In contrast, Figure 10(b) shows that the 850 K area in August 2010 was the lowest of all years, and similar to that in 1996 and 2002 which were years of anomalously weak vortices.

Further information on Antarctic atmospheric conditions during 2010 can be found in World Meteorological Organisation (WMO) Antarctic Ozone Bulletins (http://www.wmo.int/pages/prog/arep/gaw/ozone/index.html), Winter Bulletins of the National Oceanic and Atmospheric Administration (NOAA; http://www.cpc.noaa.gov/products/stratosphere/winter_bulletins), upper-air summaries of the National Climate Data Center (NCDC; http://www.ncdc.noaa.gov/sotc/upper-air) and the NOAA/NCDC State of the Climate Report (http://www.ncdc.noaa.gov/bams-state-of-the-climate; Blunden et al. 2011).

Fig. 9 Southern hemisphere vortex area evaluated on potential temperature surfaces of (a) 450 K (~18 km height) and (b) 850 K (~31 km height). The time-series for 2010 is shown in black; the blue time-series is the mean for 1992–2010, while the lower and upper red time-series in each graph show the 5th and 95th percentiles, respectively, for 1992–2010. The vortex area is evaluated using data from the United Kingdom Meteorological Office (UKMO) stratospheric assimilation, and represents the surface area enclosed by potential vorticity contours of (a) –30 Potential Vorticity Units (PVU; 1 PVU = 10^{-6} K m^2 kg^{-1} s^{-1}) and (b) –600 PVU.

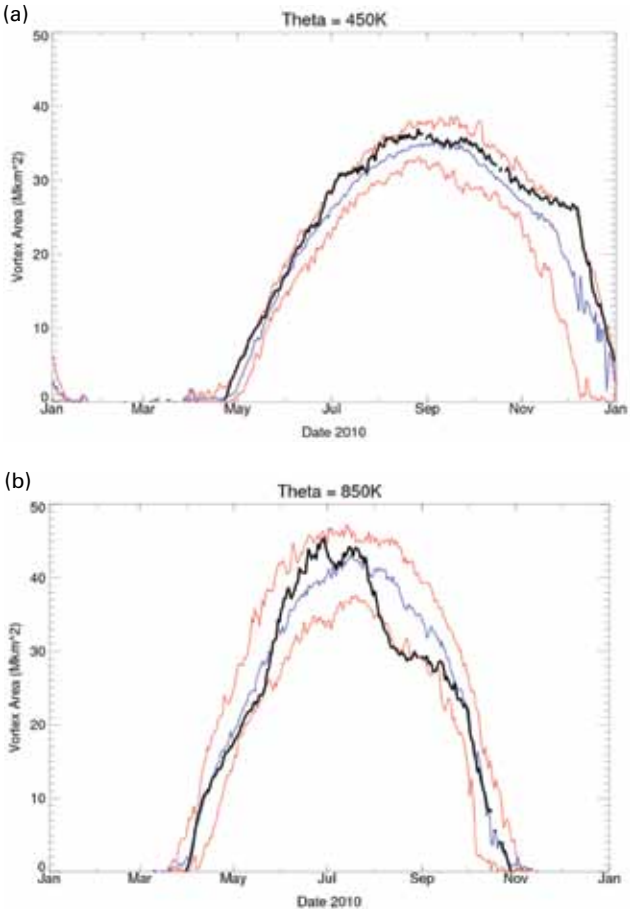

Total column ozone measurements

Ozone hole metrics

Ozone hole metrics are obtained by CSIRO using total column ozone data from the Ozone Monitoring Instrument (OMI) on board the Aura spacecraft and the Total Ozone Mapping Spectrometer (TOMS) instruments on the Earth probe and earlier spacecraft. The data discussed in this section have been processed with the NASA TOMS Version 8.5 algorithm.

Figures 11(a), 11(b) and 11(c) show timeseries of daily satellite-derived total column minima, 220 Dobson Unit (DU) ozone hole area and 220 DU referenced mass deficit, respectively, for selected years as well as individual long-term climatologies. The OMI data for 2011 presented in Fig.11(a) show that the daily ozone minimum generally

fluctuated about the climatological mean up until mid-September, after which values were below average for the rest of the year. In particular, record low values were set for two weeks around mid-December.

Figure 11(b) shows that growth of the 2010 ozone hole started late compared with recent years, and particularly so compared to 2002 which was a year in which the stratosphere was unusually warm and the vortex was anomalously weak and unstable. A general levelling of growth occurred in early September and this coincided with a reduction of the 450 K vortex area as shown in Fig. 9(a), and the stratospheric warming episode discussed in the previous section. The persistence of the ozone hole in December was also unusual, and this is associated with the low December minima noted above in relation to Fig. 11(a).

In terms of ozone hole mass deficit, the 2010 ozone hole as shown in Fig. 11(c) was modest compared with recent years, with a peak value similar to 2004 and with notably delayed growth but long persistence.

Fig. 10 Monthly averages of daily Southern Hemisphere vortex area on potential temperature surfaces of (a) 450 K for December and (b) 850 K for August, obtained using data and methods described in Fig. 9.

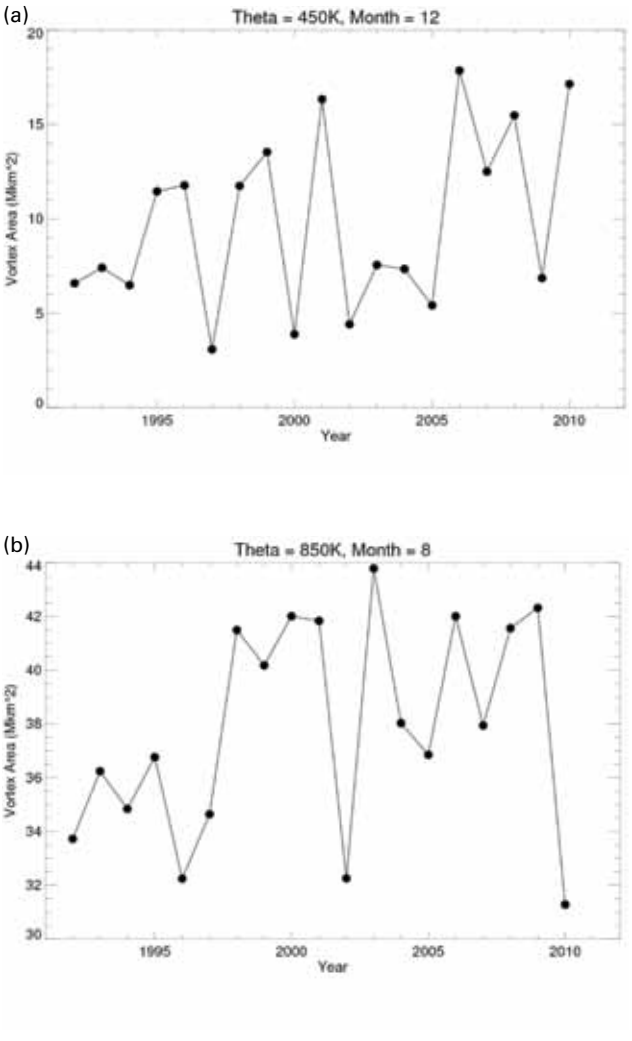

Ozone hole metric summary and rankings

Based on the ozone metrics discussed above, the 2010 ozone hole was one of the smallest in the past fifteen–twenty years. Of the 31 ozone holes for which data are available since 1979, the 2010 ozone hole ranked as follows:

Fig. 11 Estimated daily (a) ozone hole depth, (b) ozone hole area and (c) ozone mass deficit based on OMI satellite data. The 2002 and 2004 data in the above figures are from the TOMS satellite instrument.

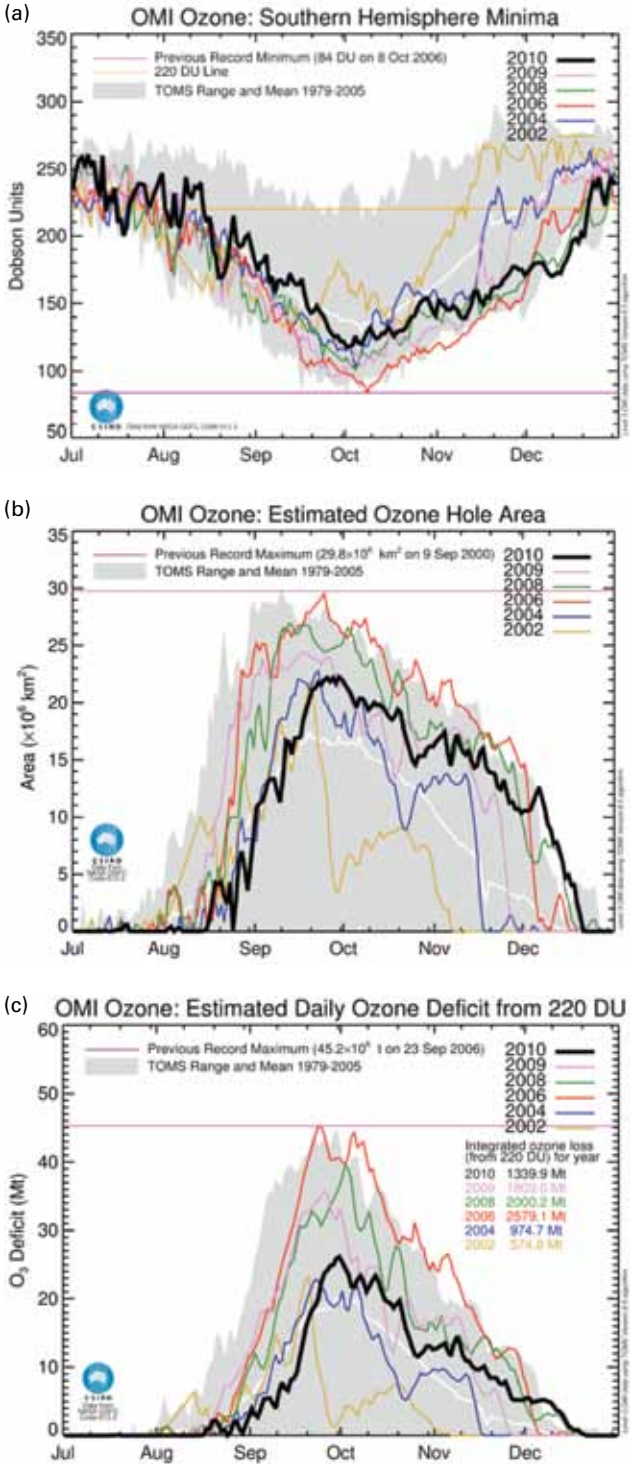

- 3rd. Latest date of ozone hole disappearance (day 355);
- 16th. 15-day average area (21.6 x10^6 km^2);
- 20th. 15-day average minimum ozone (123.9 Dobson Units (DU));
- 19th. Daily maximum area (22.2x10^6 km^2);
- 20th. Daily minimum ozone (118 DU);
- 18th. Daily maximum ozone deficit (26.1 Mt);
- 18th. Daily minimum average ozone amount in the ozone hole (164.7 DU); and
- 17th. Cumulative ozone loss (1340 Mt).

The 2010 hole can be classified as a late-starter, delayed by the stratospheric warming events of July–August and early September. These events ameliorated a much deeper ozone hole from occurring. However ozone recovery in October–December was protracted, with characteristics similar to previous large ozone holes.

Halley total column ozone

Figure 12 shows daily timeseries of total column ozone at Halley, Antarctica (75.5°S, 26.5°W) during 2010. The total column ozone measurements at Halley provide the most comprehensive such measurements in the southern hemisphere, and extend back to 1957. This station is notable in tending to lie at high equivalent latitude for much of the ozone depletion season, as the polar vortex tends to be displaced off the geographic pole and towards this sector of Antarctica. Figure 12 also shows climatological data for 1995–2010. As can be seen in Fig. 12, Halley measurements from September to mid-October 2010 were generally at the 95th percentile of the climatological data, and thus indicated relatively low ozone loss compared with the other years of the climatology. Values fluctuated about climatological mean for the remainder of the year, being generally above average from mid-October until mid-November and again in mid-December, and below average from mid-November until early December.

Fig. 12 Halley total column ozone from Dobson spectrophotometer measurements. Shown are daily values (red) for September–December 2010, and daily climatological values for 1995–2010: mean (white) and 5th to 95th percentiles (grey shaded region).

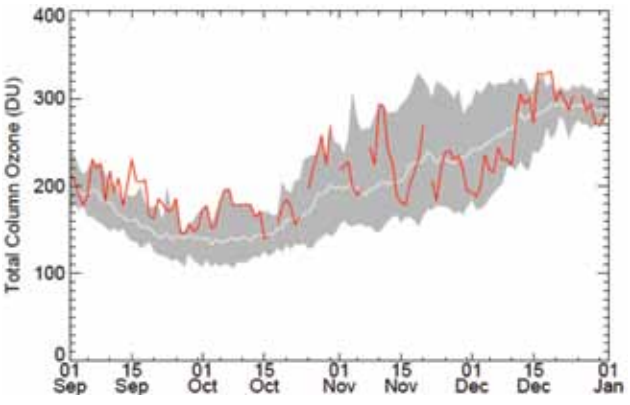

Vertically resolved ozone measurements

MLS partial columns

In Fig. 13, ozone hole area metrics are provided for three partial columns in the lower stratosphere, mid-stratosphere and full stratosphere (denoted as 'low', 'mid' and 'full' partial columns respectively) based on measurements by the Aura MLS instrument. MLS provides height-resolved ozone information during day and night, and is thus able to measure the portion of the vortex that is within continuous darkness during winter and spring and inaccessible to the OMI instrument. Figure 13 indicates that ozone depletion in the mid-stratosphere (blue time series) during late winter and early spring of 2010 was less severe and occurred later in comparison to 2009. In contrast, depletion in the lower-stratosphere (red time series) was similar for the two years. The reduced depletion in the mid-stratosphere during 2010 is likely primarily related to the effects of the stratospheric warming and disturbance to the vortex in late July and early August, and contributed to the relatively late formation of the ozone hole and a reduction in its peak size relative to 2009.

OSIRIS stratospheric ozone profiles

Vertical profiles of stratospheric ozone number density obtained from the Optical Spectrograph and Infra-Red Imager System (OSIRIS) instrument onboard the Odin satellite are presented in this section. Odin is an ongoing polar-orbiting satellite, launched in 2001, with the typical latitude coverage (in the orbit plane) from ~83°N to ~83°S. OSIRIS ozone profiles, provided since November 2001, are retrieved from the limb-scattered spectral solar irradiance

Fig. 13 Ozone hole area metrics for 2009 and 2010 derived from Aura MLS version 2.2 ozone data (Froidevaux et al. 2008) for partial columns: 146–68 hPa (red, 'low' column), 46–10 hPa (blue, 'mid' column) and 464–0.1 hPa (black, 'full' column), for which the ozone hole thresholds of 25 DU, 70 DU and 220 DU have been used, respectively. The thresholds have been chosen to enclose regions with a similar meridional gradient of ozone relative to the general level inside and outside the vortex.

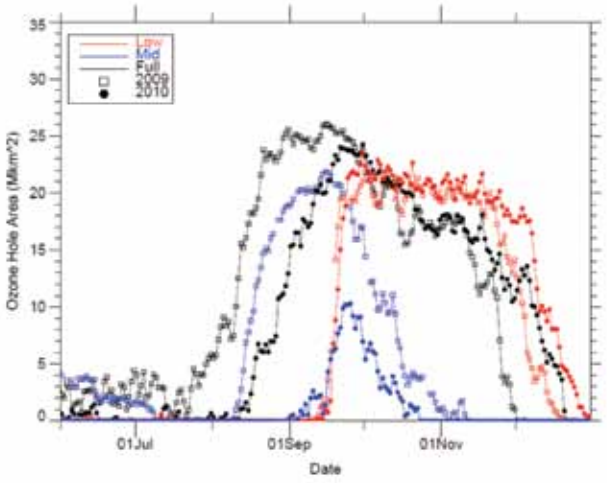

data with the 1 km vertical step. As such measurements can be obtained only in the sunlit hemisphere, the southern hemisphere data are available from late August until early March each year. The detailed instrument description and validation of OSIRIS stratospheric ozone retrievals are given in (Llewellyn et al. 2004; Petelina et al. 2004; Roth et al. 2007).

Figure 14 shows time-height sections of daily zonal mean OSIRIS ozone number density in the range 12 km to 34 km. White gaps indicate time periods when no measurements were performed. The 2002–2009 plot (Fig 14(a)) is an average of daily zonal mean ozone values over the preceding seven years. It gives a seven-year record of the onset of austral spring ozone depletion in mid-September. A clear onset of stratospheric ozone depletion is not observed in the 2010 data (Figure 14(b)) due to technical issues, particularly with measurements poleward of 70°S. For the first half of September, however, there is a clear ozone enhancement at 14–21 km height in 2010 (Fig. 14(b)) compared to a seven-year average (Fig. 14(a)). This relative increase in the spring ozone number density could be attributed to the stratospheric warming noted above, resulting in a more pronounced ozone layer for this time of year. This would also lead to a delay in the formation of the ozone hole due to a weakened polar vortex. To have a closer look at this, the 2010 daily zonal mean ozone vertical profiles were plotted for the 60°–70°S latitude range (Fig. 14(c)). As seen on this figure, at these latitudes there is still an absence of data in late September. However, in early September and through to early October, there is a clear ozone number density maximum at 17–22 km. In addition to the delay in the ozone hole formation, OSIRIS data shown in Fig. 14(b) suggest a delay in the ozone recovery until late December, which is up to four weeks later than in previous years. Comparison of vertical structure in Figs 14(a) and 14(b) suggests that in 2010, the region of ozone depletion extended about 1–2 km higher than on the seven-year average plot, and also lasted two-three weeks longer.

Fig. 14 OSIRIS daily zonal mean stratospheric ozone profiles for (a) latitudes 60°–83°S for 2002–2009, (b) 60°–83°S for 2010 and (c) 60°–70°S for 2010.

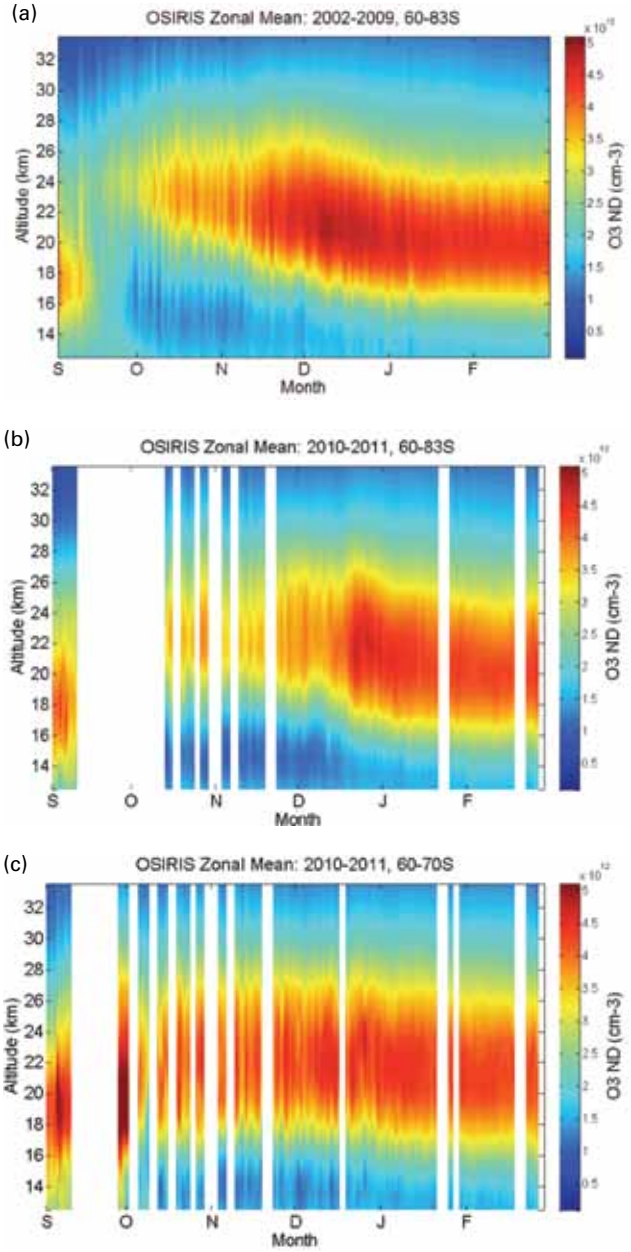

Ozonesonde measurements at Davis

Australian measurements of Antarctic ozone have been made at Davis since 2003 under a collaborative program between AAD and BoM, and these continued in 2010. A summary of the Davis ozonesonde data is presented in Fig. 15. In Fig. 15(a), the time-height evolution of ozone partial pressure is shown, revealing significant ozone depletion in the lower stratosphere (pink contours above the thermal tropopause) from late August through to the end of the year. As shown in Fig. 15(b), the 12–20 km ozone partial column derived from the ozonesonde measurements for 2010 was similar to other years, although values for September and October were generally near the upper range of all observations and similar to 2004 when a relatively small ozone hole occurred (see Fig. 11(b)).

Antarctic ultraviolet radiation

Measurements of solar ultraviolet radiation (UVR) at the Australian stations in Antarctica (Casey (66.3°S, 110.5°E), Davis (68.6°S, 78.0°E) and Mawson (67.6°S, 62.9°E)) have been made by ARPANSA, in collaboration with AAD since 1996 using broadband UVR detectors (UVBiometer Model 501, Solar Light Co., Philadelphia USA). A more detailed description of the detectors and calibration methods used by ARPANSA in Antarctica has been published previously (Tully et al. 2008).

Measurements of solar UVR utilise the UV Index (WHO, 2002), where UV Index values of two or less are low exposure risk, three to five are moderate, six to seven and eight to ten are high and very high exposure risk while eleven or more is extreme. Figure 16(a), 16(b) and 16(c) show measurements of daily UV Index for Casey, Davis and Mawson, respectively,

along with the daily total column ozone value derived from OMI satellite observations for the 2010 season. The seasonal variation of UV Index shows the effects due to changing solar zenith angle and variations in local weather conditions (cloud), with strong anti-correlation between the measured UV Index and OMI satellite measurements of total column ozone, particularly for clear sky days. Peak UV Index levels recorded at the edge of the Antarctic continent occasionally reach extreme levels when clear skies combine with low total column ozone levels.

Table 1 shows the number of days for which the total column ozone value was less than 220 DU (from OMI satellite data) for each of the Australian stations in Antarctica over the past four years, where values less than 220 DU are defined as being part of the ozone hole. While most ozone depletion events occurred in September and October for all three sites in previous years, for the first time since 2007 for Davis and since 2008 for Mawson, values less than 220 DU were recorded in December, indicating that the ozone hole event was more persistent in 2010. As with previous years, there were more ozone hole events over Mawson, where the total number of events were approximately constant, and Davis, where they increased slightly, than at Casey, where they decreased in comparison to 2008 and 2009. This

Fig. 15 Summary of ozonesonde measurements at Davis, Antarctica. (a) Time-height cross-section of ozone partial pressure. The data have been interpolated to a uniform grid with resolution 500 m (vertical) by eight days in time. (b)Time-series of partial column ozone for the height interval 12–20 km. Shown are data for all years of measurement, with data for 2010 highlighted in blue. The grey line is a climatological mean from Fortuin and Kelder (1998) interpolated to the location of Davis.

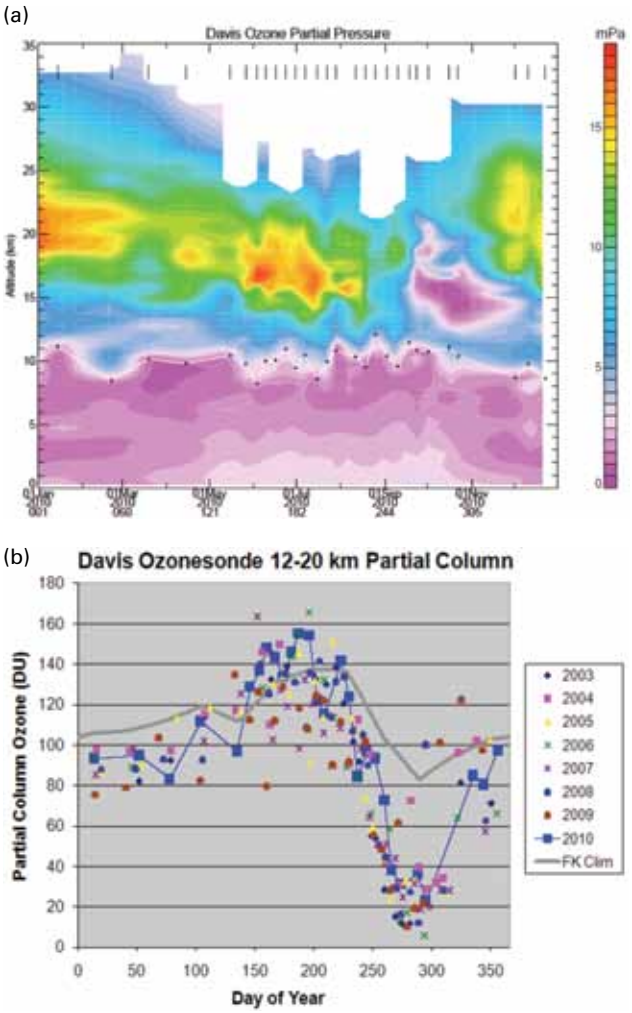

Fig. 16 Total column ozone in Dobson units (left axis) and daily UV Index (right axis) during 2010 for (a) Casey (66.3°S, 110.5°E), (b) Davis (68.6°S, 78.0°E), and (c) Mawson (67.6°S, 62.9°E). Also shown is the line for 220 Dobson units, where ozone values lower than this are defined as being part of the ozone hole (left axis).

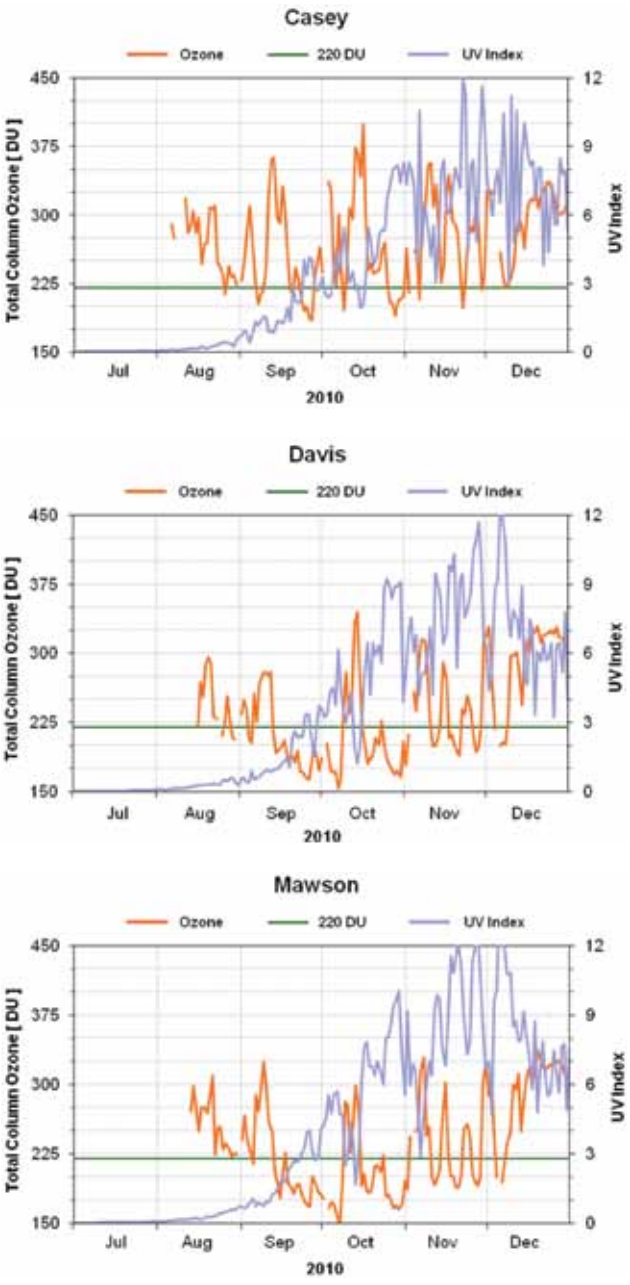

is mostly due to the asymmetry of the ozone hole and the fact that as it rotates it generally spends less time on average over the edges of Antarctica in the vicinity of Casey.

Table 2 shows the monthly mean UV Index recorded at each of the Australian stations in Antarctica over the past four years. The volatility of the UV Index on a daily basis due to rapidly changing ozone levels and cloud cover is dampened by looking at the monthly mean values. There is an obvious difference between the data from November and December in 2009 and the same months for 2010, which had higher mean UV Index values for all three stations. For other months and years the situation is less clear.

Table 3 lists the number of days for which the UV Index measured at each of the Australian Antarctic stations fell within the World Health Organisation exposure categories between July and December for each of the past four years. In 2010 there is a notable increase in the number of days of Extreme UV Index (11 +) at each of the stations compared with the previous two years. Typically the maximum UV Index for the season is recorded in early November, but for 2010 it occurred much later. The persistence of the 2010 ozone hole led to extreme UV Index values (> 11) being recorded at all stations in December, with UV Index values of 12 for Davis (6–7 Dec), 13 for Mawson (5–6 Dec) and 11.2 for Casey (10 Dec).

Table 1. Number of ozone hole events (defined as less than 220 DU) by month for the past four years over each of the Australian Antarctic stations.

	Casey				*Davis*				*Mawson*			
Month	2007	2008	2009	2010	2007	2008	2009	2010	2007	2008	2009	2010
Jul	0	0	0	0	0	0	0	0	0	0	0	0
Aug	2	5	8	1	3	2	6	3	7	6	8	0
Sep	3	11	9	10	15	21	20	20	17	21	21	18
Oct	0	7	9	7	20	17	26	22	23	20	29	23
Nov	4	4	4	4	10	9	2	13	8	11	1	14
Dec	0	0	0	0	5	0	0	4	4	1	0	3
All	9	27	30	22	53	49	54	62	59	59	59	58

Table 2: Monthly mean UV Index for the past four years measured at each of the Australian Antarctic stations. No data is available for December 2007 at Mawson.

	Casey				*Davis*				*Mawson*			
Month	2007	2008	2009	2010	2007	2008	2009	2010	2007	2008	2009	2010
Jul	0.1	0.1	0.1	0.0	0.0	0.0	0.0	0.0	0.0	0.0	0.1	0.0
Aug	0.4	0.4	0.5	0.2	0.3	0.3	0.3	0.2	0.3	0.4	0.4	0.3
Sep	1.0	2.3	1.6	1.9	1.6	2.0	1.5	1.5	1.5	2.3	1.8	1.9
Oct	3.2	4.1	4.4	4.6	4.5	4.4	6.0	5.3	5.2	5.8	7.1	6.0
Nov	6.3	5.9	5.9	7.2	7.2	7.0	4.9	7.7	6.3	7.6	5.2	8.5
Dec	6.7	6.9	6.0	7.3	7.4	6.9	6.2	6.8	n/a	8.1	7.2	8.0
All	2.7	3.3	3.1	3.5	3.4	3.4	3.2	3.6	2.6	4.1	3.6	4.1

Table 3: Number of days where the UV Index falls in each exposure category for the past four years (July to December) measured at each of the Australian Antarctic stations.

	Casey				*Davis*				*Mawson*			
UV level	2007	2008	2009	2010	2007	2008	2009	2010	2007	2008	2009	2010
Low	91	87	101	87	90	84	93	90	88	76	87	82
Moderate	21	46	36	43	38	41	41	34	33	33	34	27
High	19	28	29	22	24	35	34	28	21	31	30	31
Very High	13	21	17	26	23	23	16	27	9	38	30	30
Extreme	0	1	1	6	4	1	0	5	0	3	1	14
All	144	183	184	184	179	184	184	184	151	181	182	184

Conclusions

We have examined meteorological conditions and ozone concentrations in the Antarctic atmosphere during 2010 using a variety of data sources, including meteorological assimilations, satellite remote sensing measurements, and ground-based instruments and ozonesondes. In summary, the 2010 Antarctic ozone hole was one of the smallest in the past fifteen to twenty years. This is primarily attributed to strong planetary wave disturbances in the southern hemisphere extratropics during July and early August which produced relatively warm temperatures in the Antarctic lower stratosphere through poleward heat transport, and resulted in the off-pole displacement and weakening of the upper levels of the stratospheric polar vortex. A similar conclusion has been reached by de Laat and van Weele (2011). The development of the dynamical activity was likely influenced by the phase of the QBO which favoured poleward ducting of planetary waves and weakening of the polar vortex up to the middle of winter. The weakening of the upper part of the vortex likely increased the ozone overburden by reducing the dynamical barrier to the influx of ozone-rich air from lower latitudes, which helped to delay the development and eventual size of the ozone hole as registered by metrics based on total column ozone. Planetary wave activity in September also influenced initial growth of the ozone hole.

Notably, the polar vortex became more stable in October with less dynamical disturbance. At this time, the QBO moved into a strong positive phase that potentially favoured greater persistence of the vortex. The timing of the change in the QBO phase may have contributed to the ozone hole having an unusually late breakup date. The persistence of the vortex resulted in unusually low ozone levels into December, with relatively high UV indices measured at the Australian stations in coastal East Antarctica.

The influence of the delay in ozone recovery and persistence of the polar vortex on the meteorology of the lower atmosphere during the 2010–11 austral summer is worthy of further investigation. The QBO and surface SAM indices were both positive from October to December (Fig. 1) and from January to March 2011 (not shown), suggesting the possibility of a modifying influence at the Antarctic surface from the stratospheric conditions in late 2010.

Acknowledgments

We acknowledge the Department of Sustainability, Environment, Water, Population and Communities for support of this work. We also acknowledge the assistance of the following people: Jeff Ayton and the Australian Antarctic Division's Antarctic Medical Practitioners in collecting the solar UV data; Jeff Cumpston for obtaining lidar measurements; BoM observers for collecting upper air measurements; and for expeditioners of the British Antarctic Survey for collecting the Halley measurements. The OSIRIS operation and data retrievals are primarily supported by the Canadian Space Agency. Odin is currently a third-party mission for the European Space Agency. The OMI ozone data are courtesy of the Ozone Processing Team at NASA Goddard Space Flight Center. Aura/MLS data used in this study were acquired as part of the NASA's Earth-Sun System Division and archived and distributed by the Goddard Earth Sciences (GES) Data and Information Services Center (DISC) Distributed Active Archive Center (DAAC). UKMO data were obtained from the British Atmospheric Data Centre (http://badc.nerc.ac.uk). NCEP Reanalysis-2 data were obtained from the National Oceanic and Atmospheric Administration Earth System Research laboratory, Physical Sciences Division. Halley ozone data were made available by the British Antarctic Survey at http://www.antarctica.ac.uk/met/jds/ozone/

References

Alexander, S.P., Klekociuk, A.R., Pitts, M.C., McDonald, A.J., and Arevalo-Torres, A. 2011. The effect of orographic gravity waves on Antarctic polar stratospheric cloud occurrence and composition, *J. Geophys. Res., 116,* D06109, doi:10.1029/2010JD015184.

Arblaster, J.M., Meehl, G.A. and Karoly D.J. 2011. Future climate change in the Southern Hemisphere: Competing effects of ozone and greenhouse gases, *Geophys. Res. Lett., 38,* L02701, doi:10.1029/2010GL045384.

Baldwin, M.P. and Dunkerton, T.J. 1998. Quasi-biennial modulations of the Southern Hemisphere stratospheric polar vortex, *Geophys. Res. Lett., 25,* 3343–3346.

Baldwin, M.P. and Dunkerton, T.J. 2001. Stratospheric harbingers of anomalous weather regimes. *Science, 294,* 581–4.

Blunden, J.D., Arndt, S. and Baringer, M.O. Eds. 2011. State of the Climate in 2010. *Bull. Amer. Meteorol. Soc., 92,* S1–S266.

de Laat, A.T.J. and van Weele, M. 2011. The 2010 Antarctic ozone hole: Observed reduction in ozone destruction by minor sudden stratospheric warmings. *Sci. Rep. 1, 38;* DOI:10.1038/srep00038.

Deushi, M. and Shibata, K. 2011. Impacts of increases in greenhouse gases and ozone recovery on lower stratospheric circulation and the age of air: Chemistry-climate model simulations up to 2100, *J. Geophys. Res., 116,* D07107, doi:10.1029/2010JD015024.

Farman, J.C., Gardiner, B.G. and Shanklin, J.D. 1985. Large losses of total ozone in Antarctica reveal seasonal ClOx/NOx interaction, *Nature, 315,* 207–10.

Forster, P.M. and Thompson, D.J.W (Coordinating Lead Authors), Baldwin, M.P., Chipperfield, M.P., Dameris, M., Haigh, J.D., Karoly, D.J., Kushner, P.J., Randel, W.J., Rosenlof, K.H., Seidel, D.J., Solomon, S., Beig, G., Braesicke, P., Butchart, N., Gillett, N.P., Grise, K.M., Marsh, D.R., McLandress, C., Rao, T.N., Son, S.-W., Stenchikov, G.L. and Yoden, S. 2011. Stratospheric changes and climate, Chapter 4 in *Scientific Assessment of Ozone Depletion: 2010,* Global Ozone Research and Monitoring Project–Report No. 52, 516 pp., World Meteorological Organization, Geneva, Switzerland, 2011.

Fortuin, J.P.F and Kelder, H. 1998. An ozone climatology based on ozonesonde and satellite measurements, *J. Geophys. Res. 103,* 31709–31734.

Froidevaux, L., Jiang, Y.B., Lambert, A., Livesey, N.J., Read, W.G., Waters, J.W., Browell, E.V., Hair, J.W., Avery, M.A., McGee, T.J., Twigg, L.W., Sumnicht, G.K., Jucks, K.W., Margitan, J.J., Sen, B., Stachnik, R.A., Toon,G.C., Bernath, P.F., Boone, C.D., Walker, K.A., Filipiak, M.J., Harwood, R.S., Fuller, R.A., Manney, G.L., Schwartz, M.J., Daffer, W.H., Drouin, B.J., Cofield, R.E., Cuddy, D.T., Jarnot, R.F., Knosp, B.W., Perun, V.S., Snyder, W.V., Stek, P.C., Thurstans, R.P., and Wagner, P.A. 2008. Validation of Aura Microwave Limb Sounder stratospheric ozone measurements, *J. Geophys. Res., 113,* D15S20, doi:10.1029/2007JD008771.

Gillett, N.P., Scinocca, J.F., Plummer, D.A. and Reader, M.C. 2009. Sensitivity of climate to dynamically-consistent zonal asymmetries in ozone, *Geophys. Res. Lett., 36,* L10809, doi:10.1029/2009GL037246.

Hassler, B., Bodeker, G.E., Solomon, S. and Young, P.J. 2011. Changes in the polar vortex: Effects on Antarctic total ozone observations at various stations, *Geophys. Res. Lett., 38,* L01805, doi:10.1029/2010GL045542.

Hu, Y., Xia, Y., and Fu, Q. 2011. Tropospheric temperature response to stratospheric ozone recovery in the 21st century, *Atmos. Chem. Phys., 11,* 7687–7699, doi:10.5194/acp-11-7687-2011.

Kanamitsu, M., Ebisuzaki, W., Woollen, J., Yang, S.-K., Hnilo, J.J., Fiorino, M. and Potter, G.L. 2002. NCEP-DEO AMIP-II Reanalysis (R-2). *Bull. Am. Meteorol. Soc., 83,* 1631–1643.

Kang, S., Polvani, L.M., Fyfe, J.C. and Sigmond, M. 2011. Impact of polar ozone depletion on subtropical precipitation, *Science, 332,* 951–954.

Karpechko, A.Y., Gillett, N.P., Gray, L.J. and Dall'Amico, M. 2010, Influence of ozone recovery and greenhouse gas increases on Southern Hemisphere circulation, *J. Geophys. Res., 115,* D22117, doi:10.1029/2010JD014423.

Kawa, S.R., Stolarski, R.S., Newman, P.A., Douglass, A.R., Rex, M., Hofmann, D.J., Santee, M.L., and Frieler, K. 2009. Sensitivity of polar stratospheric ozone loss to uncertainties in chemical reaction kinetics, *Atmos. Chem. Phys., 9,* 8651–8660, doi:10.5194/acp-9-8651-2009.

Kirkwood, S., Nilsson, H., Morris, R.J., Klekociuk, A.R., Holdsworth, D.A., and Mitchell, N.J. 2008. A new height for the summer mesopause: Antarctica, December 2007, *Geophys. Res. Lett., 35,* L23810, doi:10.1029/2008GL035915.

Kirner, O., Ruhnke, R., Buchholz-Dietsch, J., Jöckel, P., Brühl, C., and Steil, B. 2011. Simulation of polar stratospheric clouds in the chemistry-climate-model EMAC via the submodel PSC, *Geosci. Model Dev., 4,* 169–182, doi:10.5194/gmd-4-169–2011.

Khosrawi, F., Urban, J., Pitts, M.C., Voelger, P., Achtert, P., Kaphlanov, M., Santee, M.L., Manney, G.L., Murtagh, D., and Fricke, K.-H. 2011. Denitrification and polar stratospheric cloud formation during the Arctic winter 2009/2010, *Atmos. Chem. Phys., 11,* 8471–8487, doi:10.5194/acp-11-8471-2011.

Llewellyn, E.J., Lloyd, N.D., Degenstein, D.A., Gattinger, R.L., Petelina, S.V., Bourassa, A.E., Wiensz, J.T., Ivanov, E.V., McDade, I.C., Solheim, B.H., McConnell, J.C., Haley, C.S., von Savigny, C., Sioris, C.E., McLinden, C.A., Griffioen, E., Kaminski, J., Evans, W.F.J., Puckrin, E., Strong, K., Wehrle, V., Hum, R.H., Kendall, D.J.W., Matsushita, J., Murtagh, D.P., Brohede, S., Stegman, J., Witt, G., Barnes, G., Payne, W.F., Picha, L., Smith, K., Warshaw, G., Deslauniers, D –L., Marchand, P., Richardson, E.H., King, R.A., Wevers, I., McCreath, W., Kyrola, E., Oikarinen, L., Leppelmeier, G.W., Auvinen, H., Mégie, G., Hauchecorne, A., Lefèvre, F., de La Noë, J., Ricaud, P., Frisk, U., Sjoberg, F., von Schëele, F. and Nordh, L. 2004. The OSIRIS Instrument on the Odin spacecraft. *Can. J. Phys., 82,* 411–422.

Manney, G.L., Santee, M.L., Rex, M., Livesey, N.J., Pitts, M.C., Veefkind, P., Nash, E.R., Wohltmann, I., Lehmann, R., Froidevaux, L., Poole, L.R., Schoeberl, M.R., Haffner, D.P., Davies, J., Dorokhov, V., Gernandt, H., Johnson, B., Kivi, R., Kyro, E., Larsen, N., Levelt, P.F., Makshtas, A., McElroy, C.T., Nakajima, H., Parrondo, M.C., Tarasick, D.W., von der Gathen, P., Walker K.A. and Zinoviev, N.S. 2011. Unprecedented Arctic ozone loss in 2011, *Nature, 478,* 469–475. doi:10.1038/nature10556.

McLandress, C., Jonsson, A.I., Plummer, D.A., Reader, M.C., Scinocca, J.F., and. Shepherd, T.G. 2010. Separating the dynamical effects of climate change and ozone depletion. Part I: Southern Hemisphere stratosphere. *J. Clim., 23,* 5002–5020. doi: 10.1175/2010JCLI3586.1

McLandress, C., Shepherd, T.G., Scinocca, J.F., Plummer, D.A., Sigmond, M., Jonsson, A.I., and Reader, M.C. 2011. Separating the dynamical effects of climate change and ozone depletion. Part II: Southern Hemisphere troposphere. *J. Clim., 24,* 1850–1868. doi: 10.1175/2010JCLI3958.1

Marshall, G. J. 2003. Trends in the Southern Annular Mode from observations and reanalyses. *J. Clim., 16,* 4134–4143.

Nash, E.R., Newman, P.A., Rosenfield, J.E. and Schoeberl, M.R. 1996. An objective determination of the polar vortex using Ertel's potential vorticity, *J. Geophys. Res., 101* (D5), 9471–9478.

Petelina, S.V., Llewellyn, E.J., Degenstein, D.A., Lloyd, N.D., Gattinger, R.L., Haley, C.S., von Savigny, C., Griffioen, E., McDade, I.C., Evans, W.F.J., Murtagh, D.P. and de La Noeet, J. 2004. Comparison of the Odin/OSIRIS stratospheric ozone profiles with coincident POAM III and ozonesonde measurements, *Geophys. Res. Lett., 31,* L07105, doi:1029/2003GL019299.

Perlwitz, J., Pawson, S., Fogt, R.L., Nielsen, J.E. and. Neff W.D. 2008. Impact of stratospheric ozone hole recovery on Antarctic climate, *Geophys. Res. Lett., 35,* L08714, doi:10.1029/2008GL033317.

Pitts, M.C., Poole, L.R., Dörnbrack, A., and Thomason, L.W. 2011. The 2009–2010 Arctic polar stratospheric cloud season: a CALIPSO perspective, *Atmos. Chem. Phys., 11,* 2161–2177, doi:10.5194/acp-11-2161-2011.

Polvani, L.M., Previdi, M. and Deser, C. 2011a. Large cancellation, due to ozone recovery, of future Southern Hemisphere atmospheric circulation trends, *Geophys. Res. Lett., 38,* LO4707, doi:10.1029/2011GL046712.

Polvani, L.M., Waugh, D.W., Correa G.J.P. and Son S.-W. 2011b: Stratospheric ozone depletion: the main driver of 20th Century atmospheric circulation changes in the Southern Hemisphere, *J. Clim., 24,* 795–812.

Rienecker, M.M., Suarez, M.J., Gelaro, R., Todling, R., Bacmeister, J., Liu, E., Bosilovich, M.G., Schubert, S.D., Takacs, L., Kim, G.-K., Bloom, S., Chen, J., Collins, D., Conaty, A., da Silva, A.,Gu, W., Joiner, J., Koster, R.D., Lucchesi, R., Molod, A., Owens, T., Pawson, S., Region, P., Redder, C.R., Reichle, R., Robertson, F.R., Ruddick, A.G., Sienkiewicz, M., and Wollen, J. 2011. MERRA - NASA's Modern-Era Retrospective Analysis for Research and Applications, *J. Climate, 24,* 3624–3648, doi: 10.1175/JCLI-D-11-00015.1

Roth, C.Z., Degenstein, D.A., Bourassa, A.E. and Llewellyn, E.J. 2007. The retrieval of vertical profiles of the ozone number density using Chappuis band absorption information and a multiplicative algebraic reconstruction technique, *Can. J. Phys., 85* (11), 1225–43.

Salby, M., Titova, E. and Deschamps, L. 2011. Rebound of Antarctic ozone, *Geophys. Res. Lett., 38,* L09702, doi:10.1029/2011GL047266.

Schwartz, M.J., Lambert, A., Manney, G.L., Read, W.G., Livesey, N.J., Froidevaux, L., Ao, C.O., Bernath, P.F., Boone, C.D., Cofield, R.E., Daffer, W.H., Drouin, B.J., Fetzer, E.J., Fuller, R.A., Jarnot, R.F., Jiang, J.H., Jiang, Y.B., Knosp, B.W., Krüger, K.R.,. F. Li, J.-L Mlynczak, M.G., Pawson, S., Russell III, J.M., Santee, M.L., Snyder, W.V., Stek, P.C., Thurstans, R.P., Tompkins, A.M., Wagner, P.A., Walker, K.A., Waters, J.W., and Wu, D.L. 2008. Validation of the Aura Microwave Limb Sounder temperature and geopotential height measurements, *J. Geophys. Res., 113,* D15S11, doi:10.1029/2007JD008783.

Sigmond, M., Reader, M.C., Fyfe, J.C., and Gillett, N.P. 2011. Drivers of past and future Southern Ocean change: Stratospheric ozone versus greenhouse gas impacts, *Geophys. Res. Lett., 38,* L12601, doi:10.1029/2011GL047120.

Siskind, D.E., Eckermann, S.D., McCormack, J.P., Coy, L., Hoppel, K.W. and Baker, N.L. 2010. Case studies of the mesospheric response to recent minor, major, and extended stratospheric warmings, *J. Geophys. Res., 115,* D00N03, doi:10.1029/2010JD014114.

Son, S.-W., et al. 2010. Impact of stratospheric ozone on Southern Hemisphere circulation change: A multimodel assessment, *J. Geophys. Res., 115,* D00M07, doi:10.1029/2010JD014271.

Sonkaew, T., von Savigny, C., Eichmann, K.-U., Weber, M., Rozanov, A., Bovensmann, H. and Burrows, J.P. 2011. Chemical ozone loss in Arctic and Antarctic polar winter/spring season derived from SCIAMACHY limb measurements 2002–2009. *Atmos. Chem. Phys. Discuss., 11,* 6555–6599, www.atmos-chem-phys-discuss.net/11/6555/2011/, doi:10.5194/acpd-11-6555-2011.

SPARC (Stratospheric Processes and their Role in Climate) CCMVal (Chemistry Climate Model Validation) 2010. SPARC Report on the Evaluation of Chemistry-Climate Models, Eyring, V., Shepherd, T.G. and Waugh, D.W. (Eds.), *SPARC Report No. 5,* WCRP-132, WMO/TD-No. 1526, http://www.atmosp.physics.utoronto.ca/SPARC.

Stolarski, R.S., Krueger, A.J., Schoeberl, M.R., McPeters, R.D., Newman, P.A. and Alpert, J.C. 1986. Nimbus 7 satellite measurements of the springtime Antarctic ozone decrease, *Nature, 322,* 808–11.

Sumińska-Ebersoldt, O., Lehmann, R., Wegner, T., Grooß, J.-U., Hösen, E., Weigel, R., Volk, C.M., Borrmann, S., Rex, M., Stroh, F., and von Hobe, M. 2011. ClOOCl photolysis at high solar zenith angles: analysis of the RECONCILE self-match flight, *Atmos. Chem. Phys. Discuss., 11,* 18901–18926, doi:10.5194/acpd-11-18901-2011.

Swinbank, R., and O'Neill, A.A.1994. Stratosphere-troposphere data assimilation system. *Mon. Weather Rev., 122,* 686–702.

Tully, M.B., Klekociuk, A.R., Deschamps, L.L., Henderson, S.I., Krummel, P.B., Fraser, P.J., Shankin, J.D., Downey, A.H., Gies, H.P. and Javorniczky, J. 2008. The 2007 Antarctic Ozone Hole. *Aust. Meteorol. Mag., 57,* 279–98.

Tully, M.B., Klekociuk, A.R., Alexander, S.P., Dargaville, R.J., Deschamps, L.L., Fraser, P.J., Gies, H.P., Henderson, S.I., Javorniczky, J., Krummel, P.B., Petelina, S.V., Shanklin, J.D., Siddaway, J.M. and Stone, K.A. 2011. The Antarctic Ozone Hole during 2008 and 2009. *Aust. Met. Oceanogr. J., 61,* 77–90.

Waugh, D.W., Oman, L., Newman, P.A., Stolarski, R.S., Pawson, S., Nielsen, J.E. and Perlwitz J. 2009a. Effect of zonal asymmetries in stratospheric ozone on simulated Southern Hemisphere climate trends, *Geophys. Res. Lett., 36,* L18701, doi:10.1029/2009GL040419.

Waugh, D.W., Oman, L., Kawa, S.R., Stolarski, R.S., Pawson, S., Douglass, A.R., Newman, P.A. and Nielsen J.E. 2009b. Impacts of climate change on stratospheric ozone recovery, *Geophys. Res. Lett., 36,* L03805, doi:10.1029/2008GL036223.

WHO (World Health Organization) 2002. *Global Solar UV Index: A Practical Guide,* ISBN 92 4 159007 6, Geneva.

WMO (World Meteorological Organization) 2011a. *Scientific Assessment of Ozone Depletion: 2010,* Global Ozone Research and Monitoring Project–Report No. 52, 516 pp., World Meteorological Organization, Geneva, Switzerland.